# $HO_x$ Observation and Model Comparison during INTEX-NA 2004

Xinrong Ren*,[1] William H. Brune,[1] Jingqiu Mao,[1] Robert B. Long,[1] Robert L. Lesher,[1] James H. Crawford,[2] Jennifer R. Olson,[2] Gao Chen,[2] Melody A. Avery,[2] Glen W. Sachse,[2] Glenn S. Diskin,[2] John D. Barrick,[2] L. Greg Huey,[3] Alan Fried,[4] Ronald C. Cohen,[5] Brian Heikes,[6] Paul Wennberg,[7] Hanwant B. Singh,[8] Donald R. Blake,[9] Richard E. Shetter[10]

[1]*Department of Meteorology, Pennsylvania State University, University Park, PA, USA*

[2]*Atmospheric Science Division, NASA Langley Research Center, Hampton, VA, USA*

[3]*School of Earth and Atmospheric Sciences, Georgia Institute of Technology, Atlanta, GA, USA*

[4]*Atmospheric Chemistry Division, National Center for Atmospheric Research, Boulder, CO, USA*

[5]*Department of Chemistry and Department of Earth and Planetary Science, University of California Berkeley, Berkeley, CA, USA*

[6]*Graduate School of Oceanography, University of Rhode Island, Narragansett, RI, USA*

[7]*Division of Engineering and Applied Sciences, California Institute of Technology, Pasadena, CA, USA.*

[8]*NASA Ames Research Center, Moffett Field, CA, USA.*

[9]*Department of Earth System Science, University of California, Irvine, CA, USA.*

[10]*National Suborbital Education & Research Center, University of North Dakota, Grand Forks, ND, USA*

*Correspondence to: X. Ren (ren@essc.psu.edu)

**Submitted to Journal of Geophysical Research**
**INTEX-A/ICARTT Special Issue**

**June 30, 2006**

**Abstract.** Measurements of OH and $HO_2$ were made with our Airborne Tropospheric Hydrogen Oxides Sensor (ATHOS) as part of a much larger measurement suite from the NASA DC-8 aircraft during the Intercontinental Chemical Transport Experiment – North America (INTEX-NA) in summer 2004. This mission, which was conducted mainly over North America and the western Atlantic Ocean, was an excellent test of atmospheric oxidation chemistry in pollution plumes throughout the troposphere. The OH and $HO_2$ measurements are compared to predictions using a photochemical box model constrained by coincident measurements of long-lived tracers and physical parameters. For most of the troposphere, observed OH and $HO_2$ were less than expected from model calculations. On average OH was over-predicted by a factor of 1.7, similar to what was observed for the Transport and Chemical Evolution over the Pacific (TRACE-P), a springtime study off the coast of Asia, but different from that for the Pacific Exploratory Mission Tropical-B (PEM-TB), a tropical Pacific study, for which the observed and modeled OH generally agreed to within a factor of 1.3. These lower-than-expected OH measurements throughout much of the troposphere in northern midlatitudes have implications for global oxidation capability. In the planetary boundary layer of forested regions, the observed-to-modeled OH ratio is a strong function of isoprene, consistent with the PROPHET measurements. $HO_2$ was over-predicted by a factor of 1.3 below 8 km altitude, similar to TRACE-P, and different from PEM-TB, for which observed and modeled $HO_2$ generally agreed to within a factor of 1.3. However, above 8 km, the observed-to-modeled $HO_2$ ratio increases from ~1 at 8 km to more ~2.5 at 11 km, suggesting either the presence of an unknown $HO_x$ source or an error in the model's chemistry involving some of the other atmospheric constituents.

**Index terms:**

0365 Atmospheric Composition and Structure: Troposphere—composition and chemistry;

0368 Atmospheric Composition and Structure: constituent transport and chemistry;

0322 Atmospheric Composition and Structure: Constituent sources and sinks;

0345 Atmospheric Composition and Structure: Pollution—urban and regional;

**Keywords:**

hydroxyl radical, hydroperoxy radical, model comparison, INTEX-NA, tropospheric chemistry

## 1. Introduction

Oxidation chemistry cleanses the atmosphere of chemical emissions from Earth's surface, establishes the global ozone balance, and influences climate change. It is dominated by the hydroxyl radical, OH, but involves the hydroperoxyl radical, $HO_2$, together called $HO_x$. OH and $HO_2$ are highly reactive species that have a large impact on the atmospheric chemistry, influencing e.g. ozone production and ultrafine aerosol formation. The abundance of radicals is determined by their production rate and the amount of $NO_x$ ($NO_x$ = NO+$NO_2$) that is present [*Jaeglé et al.*, 2000]. Reactions of OH with CO and volatile organic compounds (VOCs) lead to the formation of $HO_2$ and peroxy radicals ($RO_2$). This conversion of OH is rapid; the reaction frequency, called the OH reactivity, is typically 1 $s^{-1}$ in clean environments and 5-50 $s^{-1}$ in polluted urban environments. At the same time, $HO_2$ reacts with NO, producing $O_3$, or with $O_3$, destroying $O_3$, and in the process recreates OH. This cycle between OH and $HO_2$ is usually faster than the production and loss of the sum of OH and $HO_2$. The reaction of $RO_2$ and NO leads to the formation of $HO_2$ and $NO_2$. The exact photochemistry that occurs depends mainly on the $HO_x$ production ($P(HO_x)$), $NO_x$, the OH reactivity, and the yield of $HO_2$ and $RO_2$ from hydrocarbon oxidation.

$HO_x$ has a number of sources: photolysis of $O_3$ followed by a reaction of $O(^1D)$ with $H_2O$, photolysis of formaldehyde (HCHO), hydrogen peroxide (HOOH), and methylhydroperoxide ($CH_3OOH$), as well as reactions between $O_3$ and alkenes. Its destruction is thought to be controlled by the relatively few reactions: $HO_2$+$HO_2$, $HO_2$+OH, $HO_2$+$RO_2$, and OH+$NO_2$. Understanding these $HO_x$ sources and sinks is essential to develop predictive capability of pollution's influence on the atmosphere's oxidation capacity.

Because $HO_x$ photochemistry is so fast, comparisons with box models tests the understanding. A question is: how good is the current understanding of $HO_x$ photochemistry?

While scatter plots are useful, examining the ratio of observed-to-modeled OH and $HO_2$ as a function of important variables provides even more information. The analyses of airborne tropospheric $HO_x$ measurements from several different studies have been published [e.g., *Wennberg et al.*, 1998; *Crawford et al.*, 1999; *Brune et al.*, 1998; 1999; *Tan et al.*, 2001a; *Olson et al.*, 2004; *Olson et al.*, 2006]. When all of the studies are taken together, we can reach the conclusion that OH and $HO_2$ are generally understood to within a factor of two or so.

Considering the role of OH and $HO_2$ in the production of secondary pollutants and the role of OH in the atmosphere's oxidation capacity, a factor of two is far from good enough. Emerging from $HO_x$ studies are a set of conclusions: (1) $HO_2$, and thus ozone production, is greater than expected at larger NO values, although for some studies, new information about reaction rate coefficients and products has reduced this discrepancy [*Olson et al.*, 2006]; (2) $HO_2$ and OH are larger than expected at high solar zenith angles, as in the Subsonic Assessment: Ozone and Nitrogen Oxide Experiment (SONEX); (3) the evidence for heterogeneous influence on $HO_x$ is still inconclusive [*Olson et al.*, 2004]; (4) even with highly constraining measurement suites, OH and $HO_2$ can be either significantly larger or smaller than expected in different environments and on different missions; whether this variation in agreement is due to unmeasured atmospheric constituents, instrumental drifts and changes, or differences in models, or a combination of all three is not known; (5) agreement between instruments is inconsistent from comparison to comparison [*Eisele et al.*, 2001; 2003; *Ren et al.*, 2003].

The Intercontinental Chemical Transport Experiment – North America (INTEX-NA) was an integrated field experiment performed over North America in summer of 2004. It sought to understand the transport and transformation of gases and aerosols on transcontinental/ intercontinental scales and their impact on air quality and climate. A particular focus in this study was to quantify and characterize the inflow and outflow of pollution over North America. The

main constituents of interest are ozone and precursors, aerosols and precursors, and the long-lived greenhouse gases. Details about the overview and accomplishments of INTEX-NA are described by *Singh et al.* [2006]. *In situ* sampling of a broad suite of trace gases including OH and $HO_2$ radicals, aerosols, and meteorological parameters were provided from NASA's DC-8. This paper presents $HO_x$ observation results and a steady state modeling analysis of fast photochemistry using measurements during the INTEX-NA campaign. Similarities and difference compared to the results from previous campaigns are discussed.

## 2. Experimental and Model Description

### 2.1 OH and $HO_2$ measurements

The OH and $HO_2$ radicals were measured with the Penn State ATHOS (Aircraft Tropospheric Hydrogen Oxides Sensor), which detects OH and $HO_2$ based on laser-induced fluorescence (LIF, often called the fluorescent assay by gas expansion (FAGE) originally developed by *Hard et al.* [1984]). A detailed description of the ATHOS instrument can be found elsewhere [*Faloona et al.*, 2004]; here an abbreviated description of ATHOS is given.

The air sample is drawn into a low-pressure chamber through a pinhole inlet (1.5 mm) with a vacuum pump. As the air passes through a laser beam, OH is excited by a spectrally narrowed laser with a pulse repetition rate of 3 kHz at one of several vibronic transition lines near 308 nm ($A^2\Sigma$–$X^2\Pi$, v'=0 ← v''=0). Collisional quenching of the excited state is slow enough at the chamber pressure that the weak OH fluorescence extends beyond the prompt scattering (Rayleigh and wall scattering) and is detected with a time-gated microchannel plate (MCP) detector. $HO_2$ is measured by reaction with NO followed by the LIF detection of OH. The OH and $HO_2$ detection axes are in series: OH is detected in the first axis and $HO_2$ in a second axis as reagent NO (>99%, Matheson, Twinsburg, OH, purified through Ascarite) is added to the flow

between the two axes. The OH fluorescence signal is detected 60 ns after the laser pulse has cleared in the detection cells and is recorded every 0.2 seconds. The laser wavelength is turned on and off resonance with an OH transition every 10 seconds, resulting in a measurement time resolution of 20 seconds. The OH fluorescence signal is the difference between on-resonance and off-resonance signals.

The instrument was calibrated both in the laboratory and during the field campaign. Monitoring laser power and Rayleigh scattering, laser linewidth, and laser power maintained this calibration in flight [*Faloona et al.*, 2004]. For the calibration, water vapor photolysis by 185 nm light produced OH and $HO_2$. Absolute OH and $HO_2$ mixing ratios were calculated by knowing the 185 nm flux, which is determined with a NIST-calibrated photomultiplier tube from the University of Colorado, the $H_2O$ absorption cross section, the $H_2O$ mixing ratio, and the exposure time of the $H_2O$ to the 185 nm light. The absolute uncertainty is estimated to be ±32% for both OH and $HO_2$, with a $2\sigma$ confidence level. The $2\sigma$ precisions during this campaign were about 0.01 pptv for OH and 0.1 pptv for $HO_2$, with 1 minute integration time. Further details about the calibration process may be found elsewhere [*Faloona et al.*, 2004].

### 2.2 Other Measurements on the DC-8

The payload of the DC-8 and the measured chemical species and parameters are briefly described in *Singh et al.* [2006]. During INTEX-NA, NO was measured by a commercial NO-$NO_x$ analyzer (Model TEI 42C) based on the chemiluminescence technique. The instrument was operated in NO only mode. We also had an *in-situ* NO calibration system aboard the DC-8 and did frequent NO span and background checks. The detection limit of this instrument was about 50 pptv with 1 minute integration time. Due to this relatively high detection limit, the measured NO was not used as a constraint in the model calculations.

## 2.3 Model Description

A zero-dimensional photochemical box model developed at NASA Langley Research Center was used to calculate OH, $HO_2$ and other reactive intermediates. The model has been described in detail in several previous studies [e.g., *Crawford et al.*, 1999; *Olson et al.*, 2004; *Olson et al.*, 2006]. Model calculations use the 1-min merged data set available on the INTEX-NA public data archive (ftp://ftp-air.larc.nasa.gov/pub/INTEXA/). Model calculations require a minimum set of input constraints; these include observations of $O_3$, CO, $NO_2$, NMHC, temperature, $H_2O$ (dew/frost point), pressure, and photolysis rates. For this analysis, analyzed data were limited to solar zenith angles (SZA) between 0˚ and 85˚.

In addition to the required constraints described above, when measurements were available, the model constrained the following atmospheric constituents: hydrogen peroxide (HOOH), methyl hydrogen peroxide ($CH_3OOH$), nitric acid ($HNO_3$), and peroxy acetyl nitrate (PAN). If unavailable, these species were calculated to be in diurnal photochemical equilibrium. Some special consideration for nonmethane hydrocarbons was necessary to provide complete coverage for all model calculations. Hydrocarbons were averaged between consecutive grab samples.

As in previous studies, photolysis frequencies were based on spectroradiometer measurements [Shetter and Muller, 1999]. Diurnal variation of these measured photolysis frequencies were based on clear-sky model calculations using a DISORT eight-stream implementation of the NCAR Tropospheric Ultraviolet Visible (TUV) radiative transfer code [Madronich and Flocke, 1998]. The clear sky diurnal variation from TUV was normalized such that it matched the measured photolysis frequency at the time of observation. Unmeasured photolysis frequencies were first calculated for clear sky conditions and then corrected for

ambient cloud conditions based on the ratio of measured-to-calculated photolysis frequency of $NO_2$.

The uncertainties in the modeled OH and $HO_2$ are based on the combined uncertainties of the kinetic rate coefficients, the measured chemical concentrations, and the measured and calculated photolysis frequencies. The overall uncertainties in the modeled OH and $HO_2$ are estimated with a Monte Carlo approach (as in *Carslaw et al.*, 1999). The uncertainty in this model was estimated to be ±45% for OH and ±70% for $HO_2$, with 2σ confidence.

## 3. Results and Discussion

### 3.1 $HO_x$ Observations and Comparison with the Model Calculations

Altitude profiles of observed OH and $HO_2$ spanned from a few hundred meters above the surface to almost 12 km (Figure 1). OH mixing ratios were relatively constant at 0.2 pptv at the altitudes near surface to 6 km, but then increased with altitude above 6 km, achieving a maximum of about 0.5 pptv at 12 km. $HO_2$ mixing ratios decrease as the altitude increases, with a maximum up to about 20 pptv near the surface and a minimum of about 5 pptv at the highest altitude. The greatest $HO_2$ mixing ratios, up to almost 60 pptv, were observed just above the surface over the central United States. The median $HO_2$/OH ratio drops from 120 near the surface to 12 above 10 km, driven by both the decrease in $HO_2$ and the increase in OH with altitude. At low altitudes, the spread in $HO_2$/OH is quite large – from 20 to 300 – indicating a wide range of air composition there.

Overall comparisons of observed and modeled OH and $HO_2$ show that on average the box model over-predicts both OH and $HO_2$, with a median observed-to-modeled OH ratio of 0.61 and a median observed-to-modeled $HO_2$ ratio of 0.84 (Figure 2). The comparison of observed and modeled $HO_x$ during INTEX-NA is similar to that in the Transport and Chemical Evolution over

the Pacific (TRACE-P) where the median observed-to-modeled OH is 0.71 and the median observed-to-modeled $HO_2$ is 0.81 [*Olson et al.*, 2004]. For $HO_2$, the median observed-to-modeled ratio is within the combined 2σ uncertainties of the observations and model (0.60 to 1.70); for OH, the median observed-to-modeled ratio is at the limits of the combined 2σ uncertainties (0.65 – 1.55). Observed OH and $HO_2$ exceed the modeled OH and $HO_2$ at lower mixing ratios, but are less than modeled for the larger mixing ratios. Thus a constant measurement calibration factor error or modeling error cannot account for the differences between observed and modeled $HO_x$.

### 3.2 Comparisons with Previous Studies

ATHOS has measured OH and $HO_2$ during several recent field studies. The three most recent are the Pacific Exploratory Mission Tropics – B (PEM-TB), TRACE-P, and INTEX-NA. PEM-TB was conducted in the tropical Pacific, usually in relatively clean air. In contrast, TRACE-P was conducted off the coast of Asia in air that was often quite polluted. Both occurred in spring. Both provide an interesting contrast to INTEX-NA, which was conducted either over the continental US or over the Atlantic Ocean downwind of it. Comparing the three studies allows us to find common characteristics and differences to test the understanding of regional-scale atmospheric oxidation chemistry.

The behavior of atmospheric constituents that interact with OH and $HO_2$ is quite different for the three studies (Figure 3). Carbon monoxide (CO), nitrogen oxides ($NO_x$), and $O_3$ are factors of two or more lower in PEM-TB than in TRACE-P or INTEX-NA. This difference is to be expected because the tropics have many fewer sources of pollutant emissions than the northern midlatitudes.

For TRACE-P and INTEX-NA, CO mixing ratios are similar, except at lower altitudes where pollution from Asia measured during TRACE-P contains much more CO than North American pollution measured during INTEX-NA does. The greatest difference between TRACE-P and INTEX-NA is the $NO_x$, which was 2 to 10 times larger than measured during TRACE-P. This difference is not too surprising because TRACE-P measurements were generally a few days downstream of the source of the pollution over the Asian continent, whereas the INTEX-NA measurements were made much closer to anthropogenic and convection sources of $NO_x$ [*Bertram et al.*, 2006]. This difference is most pronounced above 8 km, where $NO_x$ during INTEX-NA can be more than 1.5 ppbv.

Because the conditions among the three studies are so different, it is instructive to compare not only the absolute values of OH, $HO_2$, and the $HO_2$/OH ratio, but also the ratios of the measured-to-modeled OH, $HO_2$, and $HO_2$/OH ratio. These are plotted as a function of the controlling environmental factors altitude (Figures 4, 6, and 8) and $NO_x$ (Figure 10).

### 3.2.1. Comparison of Observed and Modeled OH

For INTEX-NA, median observed OH is about 0.8 of modeled OH near the surface and above 11 km, but is ~0.6 of modeled OH between 2 and 8 km (Figure 4). This behavior is similar to that observed in TRACE-P, except above 9 km, where the median observed-to-modeled OH ratio continues to decrease for TRACE-P. The median observed-to-modeled OH for PEM-TB is about 0.6 only below 1 km; above that, the median observed-to-modeled ratio increases monotonically to 1.3 at 12 km.

For INTEX-NA, the median observed-to-modeled OH ratio does exceed 1 on occasion. The ratio varies from less than one to more than two along several level legs above 8 km,

indicating atmospheric constituents or chemistry that is different and varying in those air parcels compared to most of the air at those altitudes.

The observed-to-modeled OH ratio is also frequently greater than one below 1 km, in the planetary boundary layer. The location of these large ratios coincides with forested regions where isoprene is abundant. The observed-to-modeled OH ratio is a strong function of isoprene. It increases slowly from 0.6 to 1 as isoprene increases from less than 10 pptv to 500 pptv. For isoprene levels exceeding 500 pptv, the observed-to-modeled OH ratio rapidly increased to ~3 (Figure 5). In the summers of 1998 and 2000, OH and isoprene measurements were made on a tower at the PROPHET site in a Michigan forest [*Tan et al.*, 2001b]. The median daytime (SZA < 60°) observed-to-modeled OH ratio depends on isoprene in a way that is consistent with and overlaps the INTEX-NA measurements.

### 3.2.2. Comparison of Observed and Modeled $HO_2$

For INTEX-NA, the observed-to-modeled $HO_2$ ratio is approximately 0.8 from near the surface up to 8 km. Above that altitude, the observed $HO_2$ increases dramatically while the modeled $HO_2$ decreases, causing the observed-to-modeled $HO_2$ ratio from 0.8 near 8 km to more than 2 above 11 km. This increase above 8 km for INTEX-NA is completely different from either PEM-TB, for which the median ratio remained approximately 1 for the entire altitude range, or TRACE-P, for which the median ratio remained approximately 0.8 for the entire altitude range. However, a subset of the TRACE-P observations that were in stratospherically influenced air have an observed-to-modeled ratio of 1.6 [*Olson et al.*, 2004], similar to what was observed more frequently in INTEX-NA. This increase in the $HO_2$ ratio for INTEX-B occurs over an altitude range where both $NO_x$ and $O_3$ generally increase compared to PEM-TB and

TRACE-P (Figure 3). Interestingly, with exception of the points near 12 km, the observed-to-modeled $HO_2$ in the stratospherically influenced air increases with increasing $O_3$ as well as $NO_x$.

A test of the $HO_2$ measurements is provided by the two independent hydrogen peroxide measurements that were on the DC-8. The reaction $HO_2+HO_2 \rightarrow HOOH+O_2$ is the only known gas-phase atmospheric HOOH source. The predominant HOOH losses are by reaction with OH and by photolysis. However, because the HOOH photochemical lifetime is ~20 hours and HOOH is highly water soluble, HOOH will not always be in steady state. Because the steady-state imbalance is driven by either incomplete production, heterogeneous loss or convective transport, measured HOOH should be less than expected compared to either the unconstrained instantaneous model or to a steady-state calculation that uses the observed OH and $HO_2$.

The two HOOH measurements are in substantial agreement (Figure 7). Between 2 km and 8 km, they agree to well within uncertainties with the unconstrained, instantaneous model and are about 1.5 times larger than the steady-state calculation that uses observed $HO_2$ and OH. Below 2 km, HOOH is likely removed by deposition on clouds drops or Earth's surface and is therefore less than expected from steady-state. Above 8 km, the HOOH measurements remain about 1.5 times the steady-state model. This consistent difference is greater than can be explained by either the $2\sigma$ uncertainties in the $HO_x$ measurements or the uncertainty in the reaction rate coefficient for $HO_2+HO_2$ alone..

On the other hand, at 8 km, the observed HOOH becomes more than five times larger than the HOOH calculated with the unconstrained model, which at these altitudes is in steady state. Thus the HOOH measurements are more consistent with a steady-state calculation that uses observed $HO_2$ and OH than they are with the unconstrained model above 8 km. This agreement gives confidence that $HO_2$ above 8 km is much greater than the predictions of either the constrained or the unconstrained model.

The large observed-to-modeled $HO_2$ ratio above 8 km is not consistent with all other measurements. At altitudes above 8 km the measured $HO_2$ seems inconsistent with observed pernitric acid ($HO_2NO_2$) and a larger photochemical sink for $HO_2NO_2$ could help to explain the discrepancy [*Kim et al.*, 2006]. This difference suggests that some problem with $HO_x$-$NO_x$ chemistry, or in the measurements of these atmospheric constituents, persist.

A difference between observed and modeled $HO_2$ indicates either an instrument calibration error, missing $HO_x$ sources or sinks in the model, or errors in the model's chemistry. Instrument calibration errors can probably not account for the large observed-to-modeled $HO_2$ ratios above 8 km, leaving problems in with model as the likely culprit.

### 3.2.3. Comparison of Observed and Modeled $HO_2$/OH

For INTEX-NA, the median observed-to-modeled $HO_2$/OH ratio is close to 1 below 7 km, but increases to exceed 2 above ~9 km (Figure 8). The largest discrepancy appeared at altitudes between 10 and 11 km, where $HO_2$/OH was under-predicted by a factor of ~2-3. This difference is driven more by the greater-than-expected $HO_2$ than by the less-than-expected OH at these altitudes.

Comparison of observed-to-modeled ratio of $HO_2$/OH in the three studies show that below 6 km, they are all close to 1, while above 6 km, the $HO_2$/OH ratios were over-predicted by up to a factor of two for PEM-TB, under-predicted for TRACE-P by as much as a factor of 1.6, and under-predicted for INTEX-NA by a factor exceeding three (Figure 8). For INTEX-NA, at the highest altitudes near 12 km, the observed-to-modeled $HO_2$/OH ratios again became closer to 1.

An observed-to-modeled $HO_2$/OH ratio that is different from 1 usually indicates that reactions and reactants that cycle $HO_x$ between OH and $HO_2$ are not being properly represented

in the model. Because the cycling from $HO_2$ to OH is usually dominated by the well-known reactions of $HO_2$ with NO and $O_3$, an $HO_2$/OH ratio greater than 1 indicates the presence of reactants or reactions with OH that are not included in the model. That the observed-to-modeled $HO_2$/OH ratio is greater than 2 suggests that more than half of the reactivity with OH is not being captured by the model.

Some measurements were made in stratosphere-influenced air during INTEX-NA. Stratosphere-influenced air can be defined as air having $O_3$ greater than ~100 ppbv, CO less than ~100 ppbv, water vapor less than 200 ppmv, and low hydrocarbon levels. Some of the stratosphere-influenced air parcels that were encountered had more ozone, less CO, and less water vapor, and less hydrocarbons, and were thus more stratosphere-influenced than others. Thus the chosen stratosphere-influenced measurements have different amounts of mixing with tropospheric air. In this stratospher-influenced air, the observed-to-modeled OH and $HO_2$ increase from ~1 at 7 km to ~2 at 10 km before decreasing again to 1 above 11 km (Figure 9). The median observed-to-modeled $HO_2$/OH ratio, on the other hand, remains very close to one for the entire altitude range of 7-12 km. This behavior is quite different from that of the tropospheric air at the same altitudes, as shown in Figure 8.

The good agreement between the observed and modeled $HO_2$/OH ratios in the stratosphere-influenced air suggests that the $HO_x$ cycling between OH and $HO_2$ is well characterized by the model. This INTEX-NA observation contrasts with the TRACE-P observation in stratosphere-influenced air, in which the mean $HO_2$/OH observed-to-modeled ratio was 1.25. For INTEX-NA stratosphere-influenced air, the greatest observed-to-modeled OH and $HO_2$ ratios occur in dry air that contains over 300 ppbv of ozone. In contrast, the observed-to-modeled ratios for OH, $HO_2$, and $HO_2$/OH are all close to 1 for the stratosphere-influenced air observed at 11.5 km. This air was encountered on a flight early in the study over

the Pacific Ocean. Analyses have not yet uncovered the reason for the good agreement between observed and modeled $HO_x$ in these air parcels and not in others.

### 3.2.4 Comparison with $HO_x$ observations in SUCCESS

The observation of the under-prediction of $HO_2$ above 8 km during INTEX-NA appears to be unique. However, similar observations were made during SUCCESS (SUbsonic aircraft; Contrails and Clouds Effect Special Study) [*Brune et al.*, 1998]. SUCCESS was mostly over the central United States during April and May, 1996 when convection and sampling convection-influenced air was common, just as occurred during INTEX-NA [*Bertram et al.*, 2006]. NO at high altitudes was enhanced in SUCCESS, just as it was in INTEX-NA. Unfortunately, the SUCCESS payload lacked measurements of important $HO_x$ source gases. In addition, SUCCESS was the first mission for ATHOS; the OH measurements have much less precision and the OH and $HO_2$ calibrations are more uncertain than for later studies. Finally, the flight tracks were generally confined to above 6 km.

None-the-less, the general behavior of OH, $HO_2$, and $HO_2$/OH during SUCCESS are quite similar to their behavior during INTEX-NA. The observed-to-modeled OH is often between 0.5 and 1, even up to 12 km, but is also 1 to 3, especially above 10 km. The observed-to-modeled $HO_2$ is generally between 1 and 4 and is greatest at the higher altitudes. As a result, the $HO_2$/OH ratio is often ~1, even at 12 km, although for several 1-minute averaged measurements, is between 1 and 2 [*Brune et al.*, 1998].

During the flight out over the Pacific Ocean on 15 May 1996, the observed-to-modeled OH and $HO_2$ between 6 and 11 km were both between 0.5 and 1; they were both approximately 1 at 12 km. The observed-to-modeled $HO_2$/OH ratio was on average ~1 up to 12 km, where it was ~1.3. The agreement between the observations and models for this flight suggests that the air

encountered on this flight was not affected by the atmospheric constituents or chemistry that was affecting the air encountered on the other flights. This situation for SUCCESS, in which the composition and chemistry of some air masses appear to be well understood while others are not is quite similar to the observations during INTEX-NA.

### 3.2.5 $NO_x$ dependence of observed and modeled OH and $HO_2$

Two dominant factors controlling the OH and $HO_2$ levels are $NO_x$ levels and $HO_x$ production rate, $P(HO_x)$. According to the expected behavior, as $NO_x$ increases, OH first increases and then, when $NO_x$ is about 1-2 ppbv, OH decreases due to reactions such as $OH + NO_2 + M \rightarrow HNO_3 + M$. For greater $P(HO_x)$, OH is higher and the peak OH moves to greater $NO_x$ [*McKeen et al.*, 1997].

Both OH and $HO_2$ qualitatively show the expected behavior as a function of NO for INTEX-NA (Figure 10), although important quantitative differences occur. For OH, the observed-to-modeled ratios for PEM-TB, TRACE-P, and INTEX-NA are fairly constant with increasing NO, even though they are less than 1 for TRACE-P and INTEX-NA. In the cleanest conditions, the ratios are close to 1 for both PEM-TB and TRACE-P. The two ratios then diverge until NO ~ 100 pptv, where they once again converge. The OH values for PEM-TB for NO > 80 pptv come from a few hours on one flight, where the DC-8 was downwind of recent convection over the Pacific Ocean.

The observed-to-modeled $HO_2$ increases from values below and near 1 to values more than 1 when NO is more than a few hundred pptv in all three studies, although the amount of change is different for the three studies. It is worth to note that the highest NO values during INTEX-NA were observed in the upper troposphere, while the highest NO values were observed in boundary layer during TRACE-P. In previous studies, it was assumed that the chemistry and

$HO_x$ sinks were understood and that the greater-than-expected $HO_2$ was due to missing $HO_x$ sources that were emitted along with the NO [see for example *Folkins et al.*, 1997; *Wennberg et al.*, 1998; *Jaeglé et al.*, 2000]. However, the greater-than-expected $HO_2$ for enhanced NO, as is seen particularly for INTEX-NA (Figure 10(b)), has been observed in many different environments [see for example *Folkins et al.*, 1997; *Faloona et al.*, 2000; *Ren et al.*, 2003]. This frequent but not universal observation of greater-than-expected $HO_2$ at enhanced NO suggests that a missing $HO_x$ sink or an error in the model chemistry is more likely causes than a missing $HO_x$ source is.

### 3.3 $HO_x$ budget calculations

Examining the $HO_x$ production and loss provides information about the balance between $HO_x$ sources and sinks. The $HO_x$ production consists of the production from the following processes: $O_3$ photolysis followed by the $O(^1D)+H_2O$ reaction, HCHO photolysis (the radical-produced pathway only), HOOH photolysis, and the ozonolysis of alkenes. $HO_x$ loss includes the OH reaction with $NO_2$ and the reactions among OH, $HO_2$ and $RO_2$. $RO_2$ was not measured and was calculated from the box model.

The main $P(HO_x)$ was the reaction $O^1D+H_2O$ below 7 km and the photolysis of HCHO above 7 km (Figure 11(a)). Photolysis of HOOH did not contribute much to the $P(HO_x)$. For the $HO_x$ loss, $HO_2$-$RO_2$ self-reactions were the main processes below 8 km and the $OH+NO_x$ reactions became the main loss processes above 8 km (Figure 11(b)).

### 3.6 Instantaneous Ozone production

The net instantaneous ozone production in the troposphere is given to a close approximation by

$$P(O_3)_{net} = P(O_3) - L(O_3) = k_{NO+HO2}\,[NO][HO_2] + \Sigma_i\, k_{NO+RO2i}\,[NO][RO_{2i}]$$
$$- k_{OH+NO2+M}\,[M][NO_2][OH] - k_{O1D+H2O}[O(^1D)][H_2O]$$
$$- k_{HO2+O3}\,[O_3][HO_2] - k_{OH+O3}[O_3][OH]$$

where $k_{NO+HO2}$, $k_{NO+RO2i}$ $k_{OH+NO2+M}$, $k_{O1D+H2O}$, $k_{HO2+O3}$, and $k_{OH+O3}$ are the rate coefficients. Vertical profiles of instantaneous $O_3$ production rates show that $O_3$ production was mainly from the $HO_2$ + NO reaction, especially at altitudes greater than 5 km (Figure 12 (a)). At altitudes around 10 km, the $O_3$ production from $RO_2$+NO only accounted for less than 10% of the total. For the $O_3$ loss rate, $O_3$ photolysis followed by the $O^1D$ + $H_2O$ reaction was the main $O_3$ loss process below 5 km, while $O_3$ reactions with OH and $HO_2$ became the main $O_3$ loss above 6 km because of low $H_2O$ mixing ratios at these altitudes (Figure 12(b)).

For the net instantaneous $O_3$ production rate, a net $O_3$ loss rate of ~0.1-0.2 ppbv $hr^{-1}$ at altitudes between 1 and 5 km was obtained. Above 9 km, a net $O_3$ production rate of ~ 0.5-1 ppbv $hr^{-1}$ was observed (Figure 12 (c)).

## 4. Summary and Conclusions

Measurements of OH and $HO_2$ were compared to the model calculations in the INTEX-NA summer 2004 campaign. This study provides an excellent opportunity to test oxidation chemistry in pollution plumes throughout the troposphere and the following conclusions can be drawn from this study.

First, for most of the troposphere, observed OH and $HO_2$ were less than expected from model calculations. On average OH was over-predicted by a factor of 1.7 and $HO_2$ by a factor of 1.3. This observed-to-modeled comparison is similar to that for TRACE-P, another mid-latitude

study, but is different from that for PEM-TB, a tropical study, for which observed and modeled $HO_2$ generally agreed to within a factor of 1.3. In contrast, above 8 km during INTEX-NA, the observed-to-modeled $HO_2$ ratio increased from about 1 at 8 km to about 3 at 11 km.

Second, the observed-to-modeled OH ratio in the planetary boundary layer in forested regions is a strong function of isoprene. It increases slowly from 0.6 to 1 as isoprene increases from less than 10 pptv to 500 pptv. For isoprene levels exceeding 500 pptv, the observed-to-modeled OH ratio rapidly increased to ~3. This isoprene dependence of observed-to-modeled OH ratio is consistent with the PROPHET measurements.

Third, consistency between observations of $HO_2$ and HOOH in the upper troposphere but inconsistency between observations of $HO_x$ and pernitric acid suggest some problem either with $HO_x$-$NO_x$ chemistry or in the measurements of these atmospheric constituents.

Fourth, $HO_x$ budget analysis shows that the main $HO_x$ sources are the $O_3$ photolysis followed by the $O^1D+H_2O$ reaction below 7 km and the photolysis of HCHO above 7 km. The main $HO_x$ sinks are the $HO_2$-$RO_2$ self-reactions below 8 km and $OH+NO_x$ reaction above 8 km.

Finally, $O_3$ budget analysis shows that a net $O_3$ loss rate of ~0.1-0.2 ppbv $hr^{-1}$ at altitudes between 1 and 5 km was obtained. Above 9 km, a net $O_3$ production rate of ~ 0.5-1 ppbv $hr^{-1}$ was obtained.

These differences between the behavior of the observed-to-modeled OH ratio for the two studies in northern midlatitudes - TRACE-P and INTEX-NA – and for the study in the tropics - PEM-TB - suggests the presence of unknown atmospheric constituents or unknown reactions with OH that are suppressing the observed OH throughout much of the troposphere at north midlatitudes. If this discrepancy is due to emission sources and not to measurement calibrations and changes in measurements calibrations from study to study, then the lifetime of gases that are

destroyed by OH, the atmosphere's oxidation capacity, and the evolution of the atmosphere's oxidation capacity will all need to be re-examined.

The greater-than-expected $HO_2$ at altitudes above 8 km suggests the presence of an unknown $HO_x$ source or an error in the model's chemistry involving some of the other atmospheric constituents. The enhanced $NO_x$ and the dominance of calculated OH + $NO_x$ reactions as $HO_x$ sinks suggest that $HO_x$-$NO_x$ chemistry is a prime suspect for the greater-than-expected $HO_2$ in this altitude region.

It is not clear if the unknown OH sink and the unknown factors affecting $HO_2$ are related. If the less-than-expected OH and greater-than-expected $HO_2$ are not measurement artifacts, then finding the causes for these differences is a high priority for understanding the global-scale tropospheric oxidation chemistry.

**Acknowledgment**

The work was supported by NASA Tropospheric Chemistry Program. The authors would like to thank the other groups for using their data in this work, as well as the DC-8 crew and support staff during the INTEX-NA preparation and deployment periods for making this work possible.

**References**

Bertram, T. H., et al. (2006), Convection and the Age of Air in the Upper Troposphere, submitted.

Brune, W.H. et al. (1998), Airborne in-situ OH and $HO_2$ observations in the cloud-free troposphere and lower stratosphere during SUCCESS, *Geophys. Res. Let.*, 25, 1701-1704.

Brune, W. H. et al. (1999), OH and $HO_2$ chemistry in the North Atlantic free troposphere, *Geophys. Res. Lett.*, 26, 3077–3080.

Carslaw, N., P. J. Jacobs, and M. J. Pilling (1999), Modeling OH, $HO_2$, and $RO_2$ radicals in the marine boundary layer 2. Mechanism reduction and uncertainty analysis, *J. Geophys. Res.*, 104, 30,257–30,273.

Crawford, J. et al. (1999), Assessment of upper tropospheric $HO_x$ source over the tropical Pacific based on NASA GTE/PEM data: Net affect on $HO_x$ and other photochemical parameters, *J. Geophys. Res.*, 104, 16,255–16,273.

Eisele, F. L., R. L. Mauldin, D. J. Tanner, C. Cantrell, E. Kosciuch, J. B. Nowak, B. Brune, I. Faloona, D. Tan, D. D. Davis, L. Wang and G. Chen (2001), Relationship between OH measurements on two different NASA aircraft during PEM Tropics B, *J. Geophys. Res.*, 106, 32,683–32,689.

Eisele, F. L. et al. (2003), Summary of measurement intercomparisons during TRACE–P, *J. Geophys. Res.*, 108, 8791, doi:10.1029/2002JD003167.

Faloona, I., *et al*. (2000), Observations of $HO_x$ and its relationship with $NO_x$ in the upper troposphere during SONEX, *J. Geophys. Res*., 105, 3771–3783.

Faloona, I. C., D. Tan, R. L. Lesher, N. L. Hazen, C. L. Frame, J. B. Simpas, H. Harder, M. Martinez, P. DiCarlo, X. Ren, W. H. Brune (2004), A laser-induced fluorescence instrument for detecting tropospheric OH and $HO_2$: Characteristics and calibration, *J. Atmos. Chem*., 47, 139–167.

Folkins, I., P. O. Wennberg, T. F. Hanisco, J. G. Anderson, R. J. Salawitch (1997), OH, $HO_2$, and NO in two biomass burning plumes: Sources of $HO_x$ and implications for ozone production, *Geophys. Res. Let.*, 24, 3185-3188.

Hard, T.M., R.J. O'Brien, C.Y. Chan and A.A. Mehrabzadeh (1984), Tropospheric free radical determination by FAGE, *Environ. Sci. Technol., 18*, 768–777.

Jaeglé, L., D. J. Jacob, W. H. Brune, I. Faloona, D. Tan, B. G. Heikes, Y. Kondo, G. W. Sachse, B. Anderson, G. L. Gregory, H. B. Singh, R. Pueschel, G. Ferry, D. R. Blake, R. E. Shetter (2000), Photochemistry of $HO_x$ in the upper troposphere at northern midlatitudes, J. Geophys. Res., 105, 3877–3892.

Kim, S. et al. (2006), Measurement of $HO_2NO_2$ in the upper troposphere during INTEX-NA 2004, submitted to J. Geophys. Res.

Madronich, S., and S. Flocke (1998), The role of solar radiation in atmospheric chemistry, in Handbook of Environmental Chemistry, edited by P. Boule, pp. 1–26, Springer, New York.

Martinez, M. et al. (2003), OH and HO2 concentrations, sources, and loss rates during the Southern Oxidants Study in Nashville, Tennessee, summer 1999, *J. Geophys. Res.*, 108, 4617, doi: 10.1029/2003JD003551.

McKeen, S. A., G. Mount, F. Eisele, E. Williams, J. Harder, P. Goldan, W. Kuster, S. C. Liu, S.C., Baumann, K., Tanner, D., Fried, A., Sewell, S., Cantrell, C., Shetter, R., 1997. Photochemical modeling of hydroxyl and its relationship to other species during the Tropospheric OH Photochemistry Experiment. Journal of Geophysical Research 102, 6467–6493.

Olson, J. R. et al. (2004), Testing fast photochemical theory during TRACE-P based on measurements of OH, $HO_2$, and $CH_2O$, *J. Geophys. Res.*, 109, D15S10, doi:10.1029/2003JD004278.

Olson, J. R., J. H. Crawford, G. Chen, W. H. Brune, I. C. Faloona, D. Tan, H. Harder, and M. Martinez (2006), A reevaluation of airborne $HO_x$ observations from NASA field campaigns, *J. Geophys. Res.*, 111, D10301, doi:10.1029/2005JD006617.

Ren, X., H. Harder, M. Martinez, R. L. Lesher, A. Oliger, J. B. Simpas, W. H. Brune, J. J. Schwab, K. L. Demerjian, Y. He, X. L. Zhou, H. G. Gao (2003), OH and $HO_2$ chemistry in the urban atmosphere of New York City, *Atmos. Environ*., 37, 3639–3651.

Shetter, R. E., and M. Muller (1999), Photolysis frequency measurements using actinic flux spectroradiometry during the PEM-Tropics mission: Instrumentation description and some results, J. Geophys. Res., 104, 5647–5661.

Singh, H. B., W. H. Brune, J. H. Crawford (2003), Reactive nitrogen and hydrogen in the global atmosphere: Progress in measurements and theory, in *Recent Advances in Atmospheric and Oceanic Sciences-Part-II: Air Pollution Studies*, Proceedings of the Indian National Science Academy, 69/6, 669-683.

Singh, H. B., W. H. Brune, J. H. Crawford, and D. J. Jacob (2006), Overview of the Summer 2004 Intercontinental Chemical Transport Experiment-North America (INTEX-A), submitted to *J. Geophys. Res.*

Tan, D., et al. (2001a), OH and $HO_2$ in the tropical Pacific: Results from PEM Tropics B, *J. Geophys. Res., 106*, 32,667–32,681.

Tan, D., I. Faloona, J. B. Simpas, W. Brune, P. B. Shepson, T. L. Couch, A. L. Sumner, M. A. Carroll, T. Thornberry, E. Apel, D. Riemer, and W. Stockwell (2001b), $HO_x$ budgets in a deciduous forest: Results from the PROPHET summer 1998 campaign, *J. Geophys. Res.*, 106, 24,407–24,427.

Wennberg, P.O., et al., (1998), Hydrogen radicals, nitrogen radicals, and the production of $O_3$ on the upper troposphere, *Science*, 279, 49-53.

**Figure captions:**

**Figure 1.** Observed OH and $HO_2$ mixing ratios and $HO_2$/OH ratio as a function of altitude during INTEX-NA. Small dots are the 1-minute averaged data; the linked circles denote median values in 0.5 km altitude bins.

**Figure 2.** Comparison of observed and modeled OH (a) and $HO_2$ (b). The solid lines indicate the 1:1 lines and the dashed lines indicate the observation uncertainty of ±32%.

**Figure 3.** Comparisons of the altitude profiles for atmospheric constituents for PEM-TB (triangles), TRACE-P (stars), and INTEX-NA (circles) for (left) CO, (middle) $NO_x$, and (right) $O_3$. Individual 1-minute measurements for INTEX-NA are shown as gray points.

**Figure 4.** Comparison of the vertical profiles of (left) measured (circles) and modeled (stars) OH and (right) measured-to-modeled OH ratios during in INTEX-NA (circles), TRACE-P (stars) and PEM-TB (triangles). Individual INTEX-NA 1-minute measurements are shown (gray dots).

**Figure 5.** The observed-to-modeled OH ratio as a function of isoprene. Individual 1-minute measurements (gray points) and median values for isoprene intervals (circles) are shown for data taken at less than 1 km altitude and solar zenith angle less than 60°. Median observed-to-modeled OH ratios from the PROPHET tower in a Michigan forest in summer 2000 are also shown (triangles).

**Figure 6.** Comparison of the vertical profiles of (left) measured (circles) and modeled (starts) $HO_2$ and (right) measured-to-modeled $HO_2$ ratios during in INTEX-NA (circles), TRACE-P (stars) and PEM-TB (triangles). Individual INTEX-NA 1-minute measurements are shown (gray dots).

**Figure 7.** Variation of median HOOH with altitude for the unconstrained instantaneous model (dotted line), the steady-state calculation using observed OH and $HO_2$ (solid line), and the

measurements of the University of Rhode Island (circles) and California Institute of Technology (stars).

**Figure 8.** Comparison of the vertical profiles of (left) measured (circles) and modeled (stars) $HO_2$/OH and (right) measured-to-modeled $HO_2$/OH during INTEX-NA (circles), TRACE-P (stars) and PEM-TB (triangles). Individual INTEX-NA 1-minute measurements are shown (gray dots).

**Figure 9.** Observed-to-modeled OH, $HO_2$, and $HO_2$/OH ratios in stratosphere-influenced air. Shown are 1-km median values (circles and lines) and individual 1-minute values (gray dots).

**Figure 10.** Comparison of $NO_x$ dependence for (a) OH and (b) $HO_2$ of (up) measured (circles) and modeled (stars) values and (down) measured-to-modeled ratios during in INTEX-NA (circles), TRACE-P (stars) and PEM-TB (triangles). Individual INTEX-NA 1-minute measurements are shown (gray dots).

**Figure 11.** Vertical median profiles of (a) $HO_x$ production: total (thick line), from $O(^1D)+H_2O$ (circles), from HCHO photolysis (stars), and from $H_2O_2$ photolysis; and (b) $HO_x$ loss rates: total (thick line), due to $HO_2+HO_2/RO_2$ (circles), due to $OH+HO_2$ (stars), and due to $OH+NO_x$ (triangles) during INTEX-NA. Small gray dots show the 1-minute data for (a) total $HO_x$ production rate, (b) total $HO_x$ loss rate.

**Figure 12.** Vertical median profiles of (a) instantaneous $O_3$ production rate: total (circles), from $HO_2+NO$ (stars), and from $RO_2+NO$ (triangles); (b) $O_3$ loss rate: total (circles), due to $O(1D)+H_2O$ (stars), due to $O_3+OH$ (triangles), and due to $O_3+HO_2$ (solid line); and (c) net $O_3$ production rate during INTEX-NA. Small gray dots show the 1-minute data for (a) total $O_3$ production rate, (b) total $O_3$ loss rate, and (c) net $O_3$ production.

**Figure 1.** Observed OH and $HO_2$ mixing ratios and $HO_2$/OH ratio as a function of altitude during INTEX-NA. Small dots are the 1-minute averaged data; the linked circles denote median values in 0.5 km altitude bins.

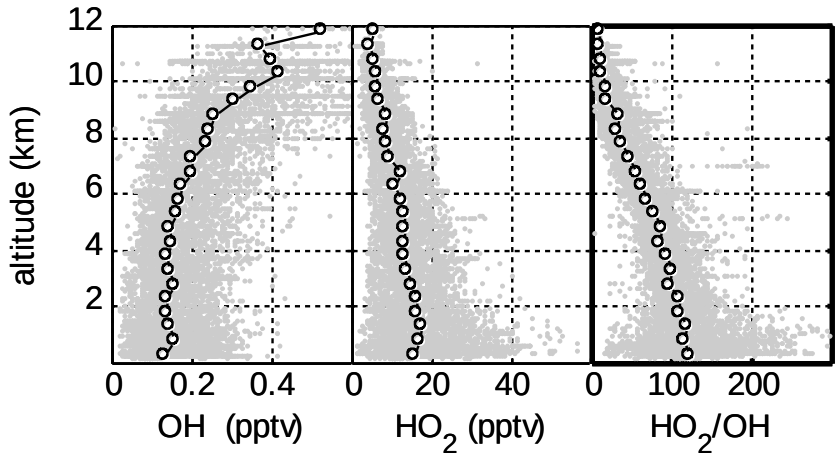

**Figure 2.** Comparison of observed and modeled OH (a) and $HO_2$ (b). The solid lines indicate the 1:1 lines and the dashed lines indicate the observation uncertainty of ±32%.

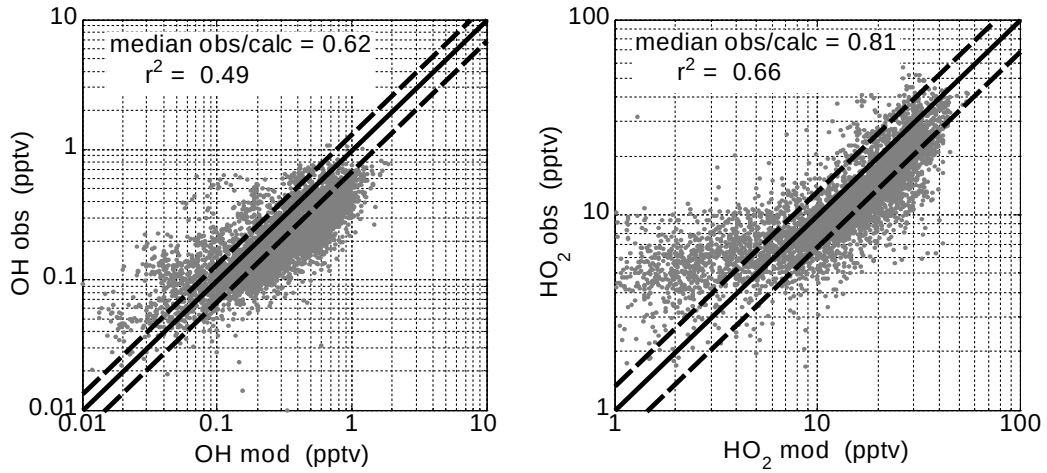

**Figure 3.** Comparisons of the altitude profiles for atmospheric constituents for PEM-TB (triangles), TRACE-P (stars), and INTEX-NA (circles) for (left) CO, (middle) $NO_x$, and (right) $O_3$. Individual 1-minute measurements for INTEX-NA are shown as gray points.

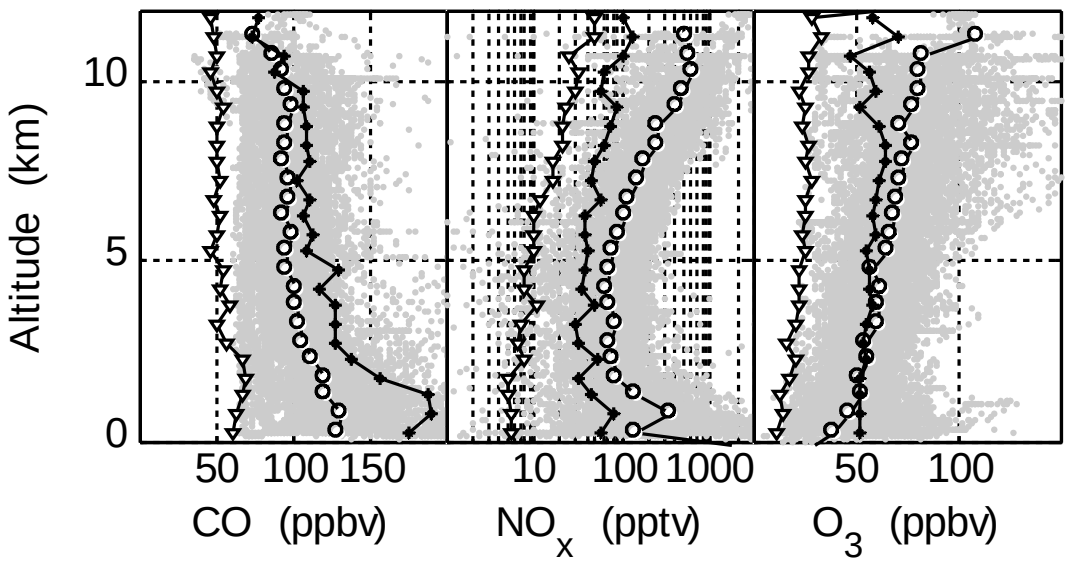

**Figure 4.** Comparison of the vertical profiles of (left) measured (circles) and modeled (stars) OH and (right) measured-to-modeled OH ratios during in INTEX-NA (circles), TRACE-P (stars) and PEM-TB (triangles). Individual INTEX-NA 1-minute measurements are shown (gray dots).

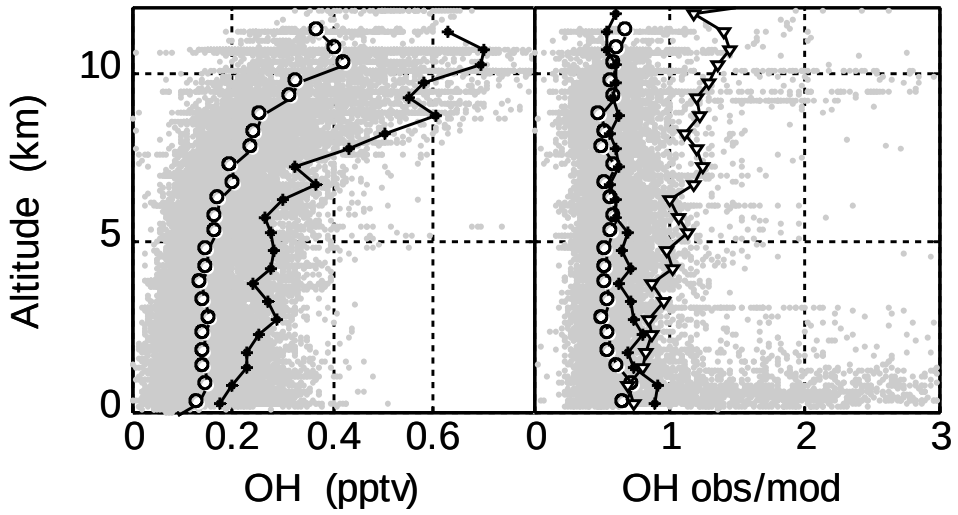

**Figure 5.** The observed-to-modeled OH ratio as a function of isoprene. Individual 1-minute measurements (gray points) and median values for isoprene intervals (circles) are shown for data taken at less than 1 km altitude and solar zenith angle less than 60°. Median observed-to-modeled OH ratios from the PROPHET tower in a Michigan forest in summer 2000 are also shown (triangles).

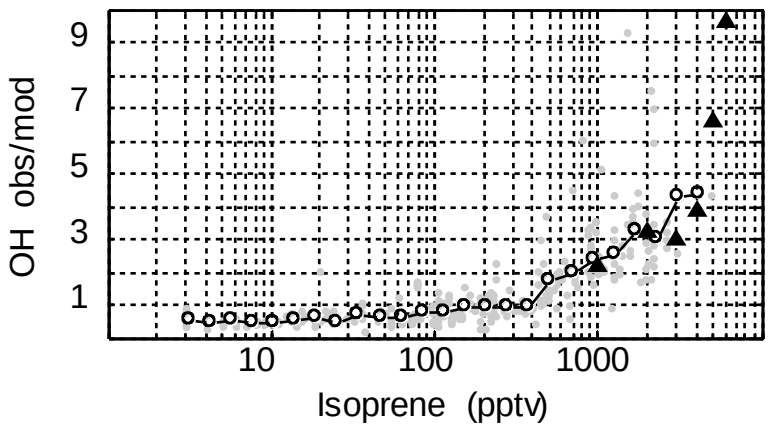

**Figure 6.** Comparison of the vertical profiles of (left) measured (circles) and modeled (starts) $HO_2$ and (right) measured-to-modeled $HO_2$ ratios during in INTEX-NA (circles), TRACE-P (stars) and PEM-TB (triangles). Individual INTEX-NA 1-minute measurements are shown (gray dots).

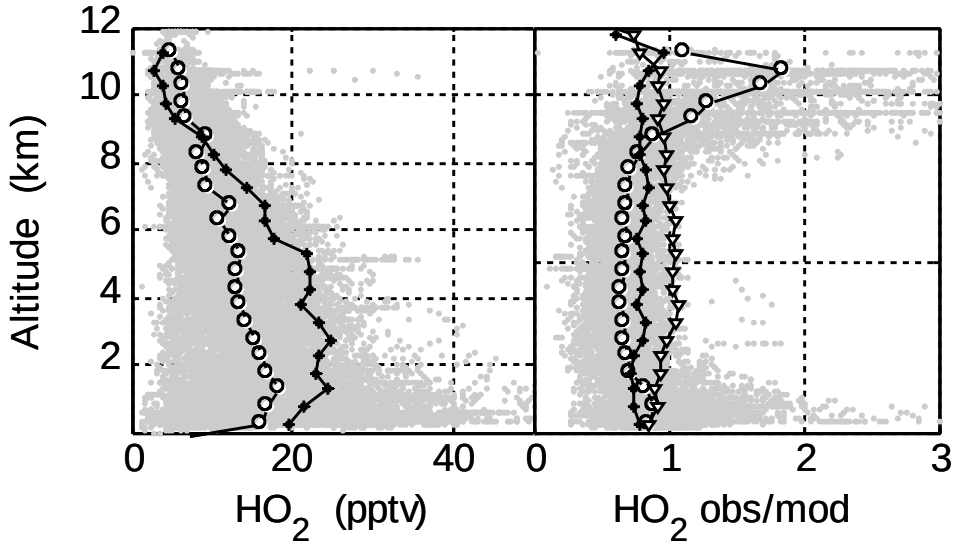

**Figure 7.** Variation of median HOOH with altitude for the unconstrained instantaneous model (dotted line), the steady-state calculation using observed OH and $HO_2$ (solid line), and the measurements of the University of Rhode Island (circles) and California Institute of Technology (stars).

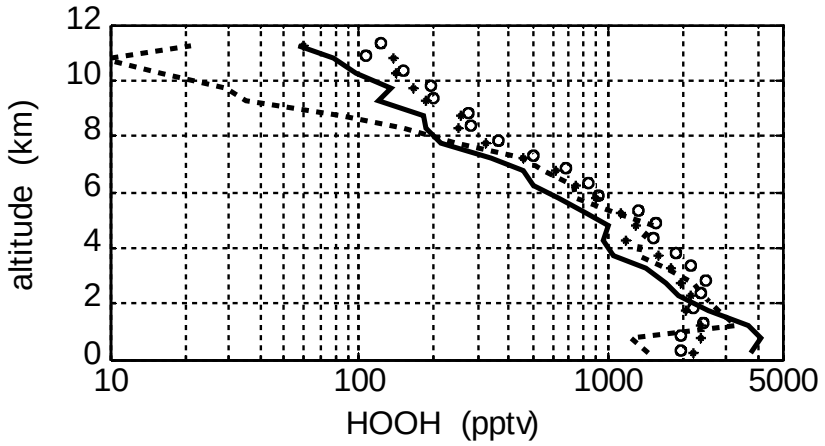

**Figure 8.** Comparison of the vertical profiles of (left) measured (circles) and modeled (stars) $HO_2$/OH and (right) measured-to-modeled $HO_2$/OH during INTEX-NA (circles), TRACE-P (stars) and PEM-TB (triangles). Individual INTEX-NA 1-minute measurements are shown (gray dots).

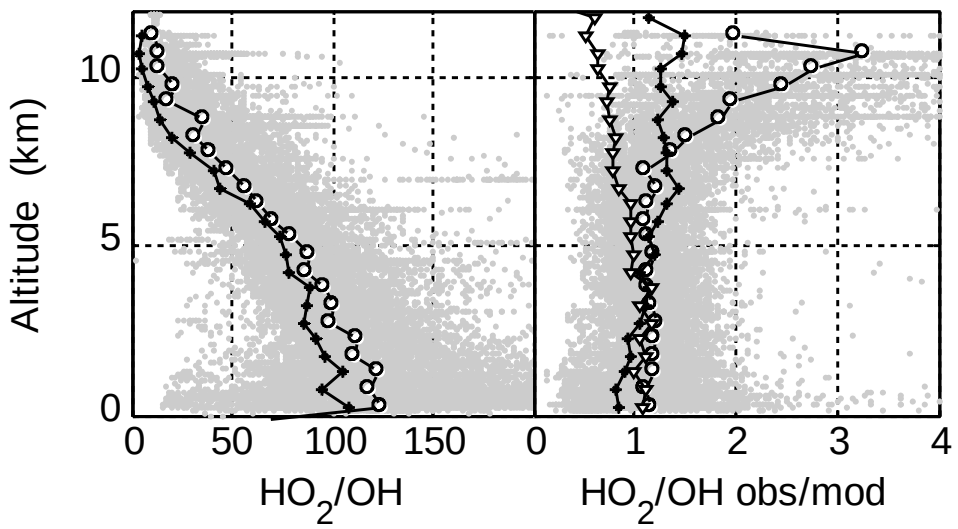

**Figure 9.** Observed-to-modeled OH, $HO_2$, and $HO_2$/OH ratios in stratosphere-influenced air. Shown are 1-km median values (circles and lines) and individual 1-minute values (gray dots).

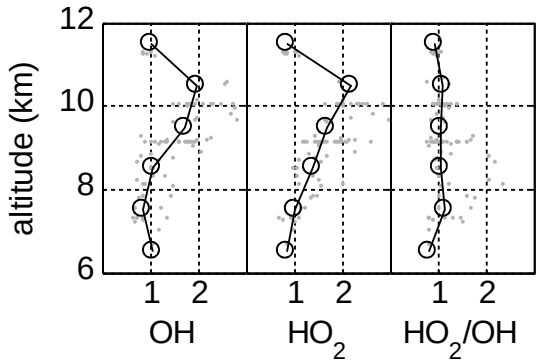

**Figure 10.** Comparison of $NO_x$ dependence for (a) OH and (b) $HO_2$ of (up) measured (circles) and modeled (stars) values and (down) measured-to-modeled ratios during in INTEX-NA (circles), TRACE-P (stars) and PEM-TB (triangles). Individual INTEX-NA 1-minute measurements are shown (gray dots).

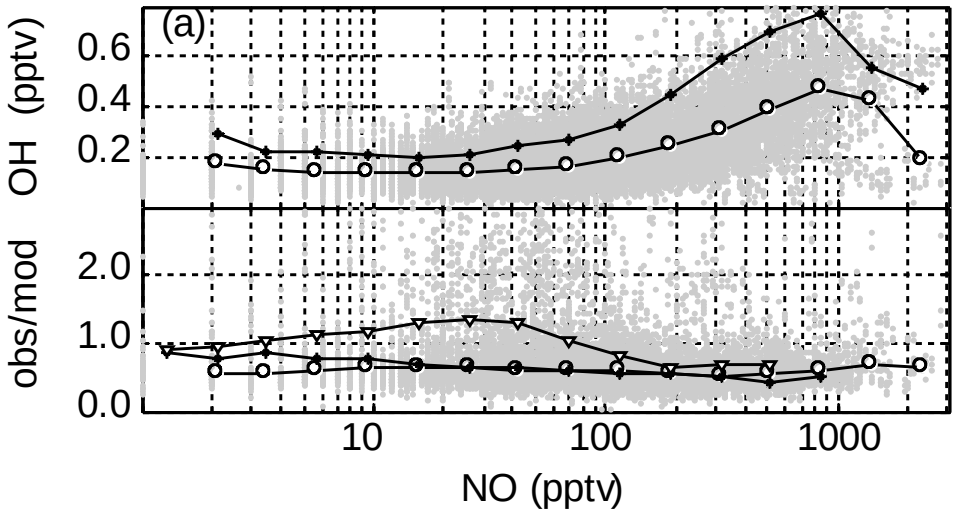

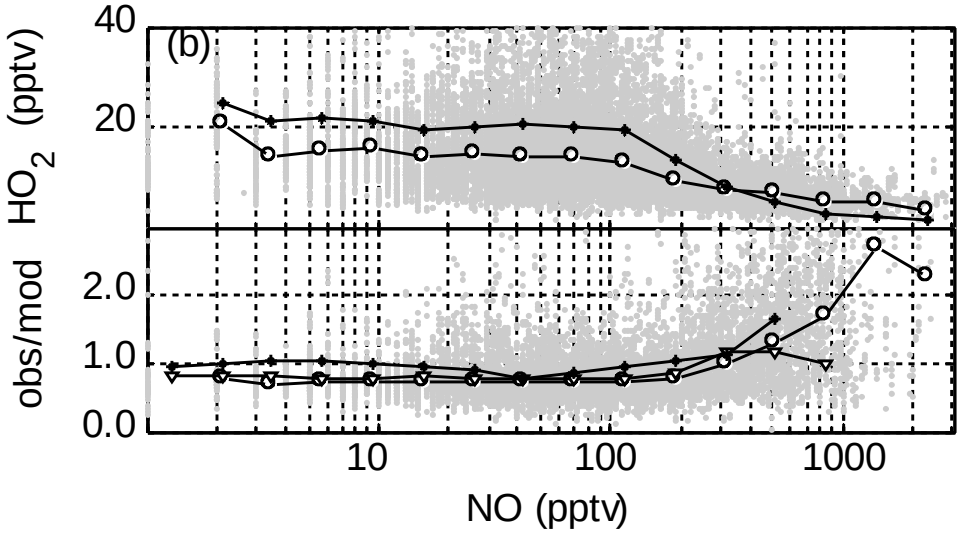
(b)
40
20
2.0
1.0
0.0
HO2 (pptv)
obs/mod
10
100
1000
NO (pptv)

**Figure 11.** Vertical median profiles of (a) $HO_x$ production: total (thick line), from $O(^1D)+H_2O$ (circles), from HCHO photolysis (stars), and from $H_2O_2$ photolysis; and (b) $HO_x$ loss rates: total (thick line), due to $HO_2+HO_2/RO_2$ (circles), due to $OH+HO_2$ (stars), and due to $OH+NO_x$ (triangles) during INTEX-NA. Small gray dots show the 1-minute data for (a) total $HO_x$ production rate, (b) total $HO_x$ loss rate.

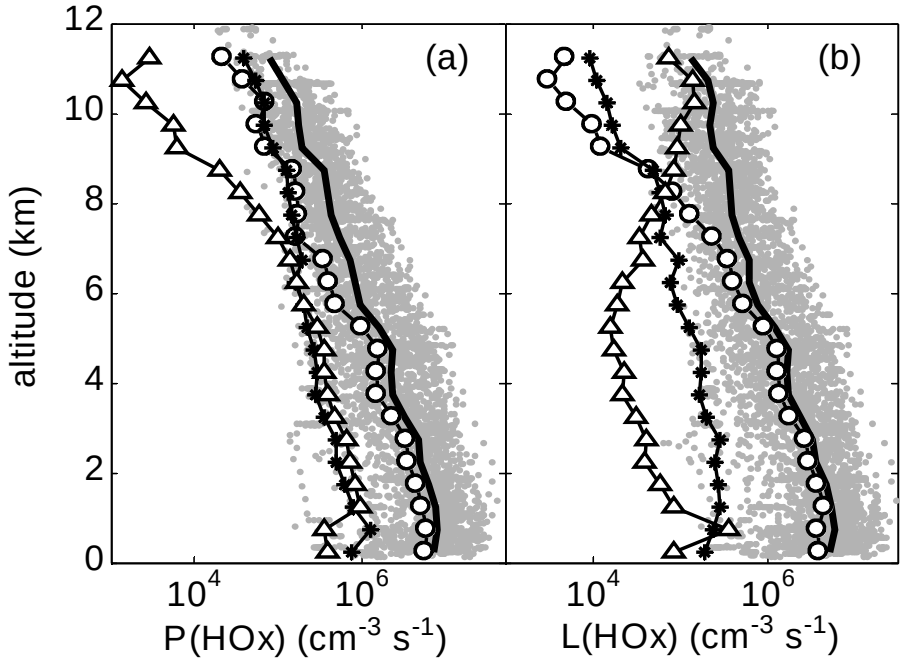
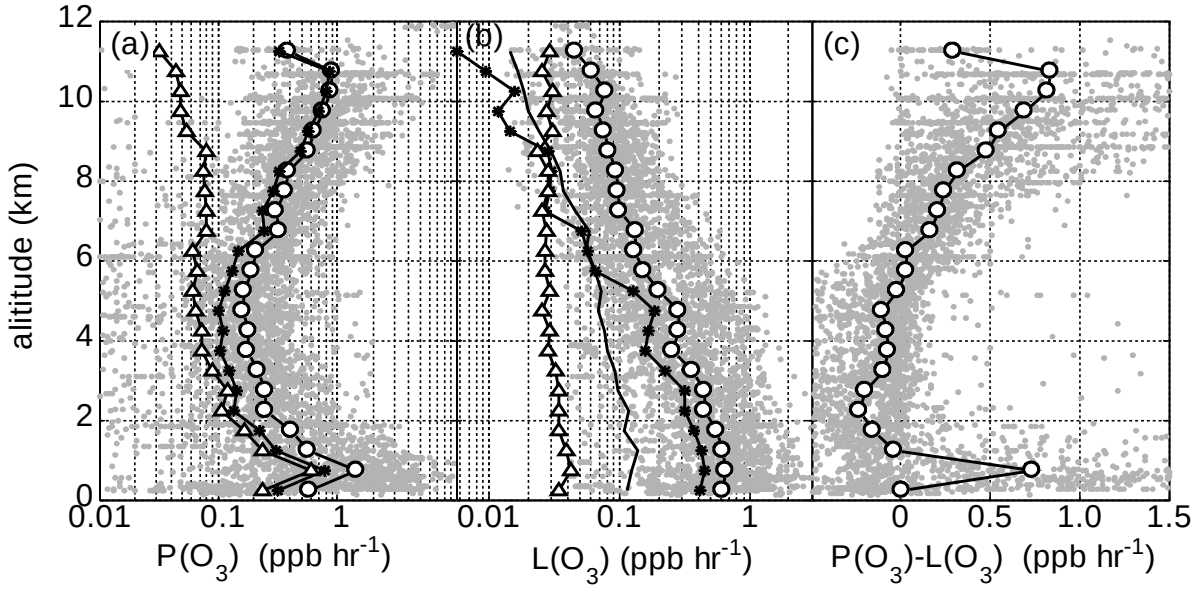
**Figure 12.** Vertical median profiles of (a) instantaneous $O_3$ production rate: total (circles), from $HO_2$+NO (stars), and from $RO_2$+NO (triangles); (b) $O_3$ loss rate: total (circles), due to O(1D)+$H_2O$ (stars), due to $O_3$+OH (triangles), and due to $O_3$+$HO_2$ (solid line); and (c) net $O_3$ production rate during INTEX-NA. Small gray dots show the 1-minute data for (a) total $O_3$ production rate, (b) total $O_3$ loss rate, and (c) net $O_3$ production.